Journal of Biomechanics 128 (2021) 110804

Contents lists available at ScienceDirect

Journal of Biomechanics

journal homepage: www.elsevier.com/locate/jbiomech

Force distribution within the frame of self-expanding transcatheter aortic valve: Insights from in-vivo finite element analysis

Tian-Yuan Xiong [a], Elisa Stoppani [b], Matthieu De Beule [b], Fei Chen [a], Yi-Jian Li [a], Yan-Biao Liao [a], Yuan Feng [a], Peter de Jaegere [c,*], Mao Chen [a,*]

[a] Department of Cardiology, West China Hospital, Sichuan University, Chengdu, China
[b] FEops NV, Technologiepark, Ghent, Belgium
[c] Department of Cardiology, Erasmus Medical Center, Rotterdam, the Netherlands

ARTICLE INFO

Keywords:
Transcatheter aortic valve replacement
Finite element analysis
Computer simulation
Force

ABSTRACT

We sought to assess the amount and distribution of force on the valve frame after transcatheter aortic valve replacement (TAVR) via patient-specific computer simulation. Patients successfully treated with the self-expanding Venus A-Valve and multislice computed tomography (MSCT) pre- and post-TAVR were retrospectively included. Patient-specific finite element models of the aortic root and prosthesis were constructed. The force (in Newton) on the valve frame was derived at every 3 mm from the inflow and at every 22.5° on each level. Twenty patients of whom 10 had bicuspid aortic valve (BAV) were analyzed. The total force on the frame was 74.9 N in median (interquartile range 24.0). The maximal force was observed at level 5 that corresponds with the nadir of the bioprosthetic leaflets and was 9.9 (7.1) N in all patients, 10.3 (6.6) N in BAV and 9.7 (9.2) N for patients with tricuspid aortic valve (TAV). The level of maximal force located higher from the native annulus in BAV and TAV patients (8.8 [4.8] vs. 1.8 [7.4] mm). The area of the valve frame at the level of maximal force decreased from 437.4 (239.7) mm^2 at the annulus to 377.6 (114.3) mm^2 in BAV, but increased from 397.5 (114.3) mm^2 at the annulus to 406.7 (108.9) mm^2 in TAV. The maximum force on the bioprosthetic valve frame is located at the plane of the nadir of the bioprosthetic leaflets. It remains to be elucidated whether this may be associated with bioprosthetic frame and leaflet integrity and/or function.

1. Introduction

At variance with surgical aortic valve replacement (SAVR), the native aortic valve is not excised during transcatheter aortic valve replacement (TAVR). During SAVR, fixation of the surgical valve consists of suturing of a (most often) rigid frame into the aortic root while during TAVR the bioprosthetic valve anchors within the aortic root due to a complex and dynamic interaction between the valve and host. Consequently, there is a continuous force between the valve frame and the anatomy. The interaction between prosthesis and anatomy is at multiple levels from the left ventricular outflow tract, aortic annulus, aortic leaflets, sinotubular junction to the initial part of the ascending aorta. The cusps have an average height of 15 mm measured on gross samples (Jatene et al., 1999), thus accounting for a large proportion of prosthesis-anatomy interaction and, hence, mutual force generation.

In practice, one may intentionally increase this force by oversizing the prothesis in regard to the aortic annulus to minimize paravalvular leak (PVL) and the risk of valve embolization (Blanke et al., 2014). However, the empirical use of aortic annulus as the major reference for sizing has been questioned (Xiong et al., 2018). Noncircular and under-expansion of the valve frame is frequent (Zegdi et al., 2008). Excessive force can also result in distortion of the bioprosthetic leaflets and abnormal kinematics, leading to hypo-attenuated leaflet thickening (Fuchs et al., 2017) and impaired durability of transcatheter aortic valves (Bailey et al., 2017; Gunning et al., 2014). A detailed analysis of the distribution of force within the valve frame is essential to further understand where the potentially vulnerable regions are located and what anatomical structures mainly exert forces to the device, but the evidence is lacking.

An analysis from multislice computed tomography (MSCT) after implantation of the cylinder-shape Lotus valve in patients with aortic stenosis has demonstrated that the anatomy restricting the valve

* Corresponding authors at: Department of Cardiology, West China Hospital, Sichuan University, #37 Guoxue Alley, Chengdu 610041, China (M. Chen). Department of Cardiology, Thoraxcenter, Erasmus Medical Center, Rotterdam, the Netherlands (P. de Jaegere).
E-mail addresses: p.dejaegere@erasmusmc.nl (P. de Jaegere), hmaochen@vip.sina.com (M. Chen).

https://doi.org/10.1016/j.jbiomech.2021.110804
Accepted 6 October 2021
Available online 11 October 2021

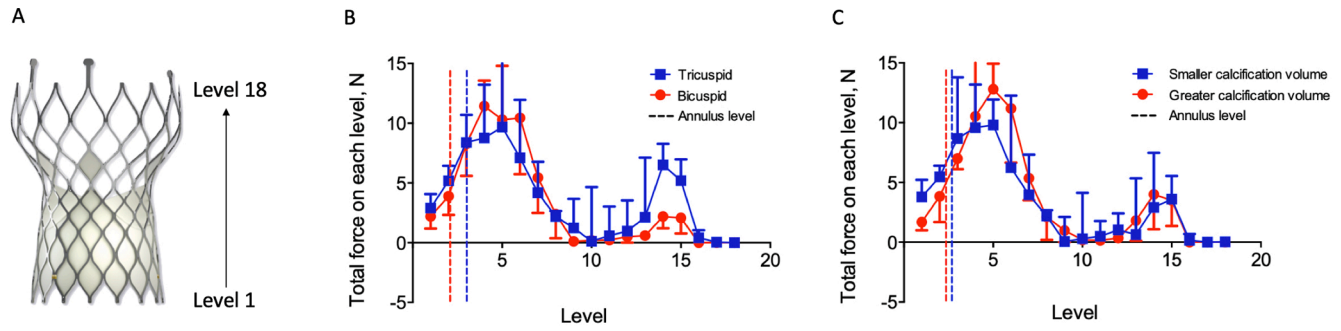

Fig. 1. Distribution of force on the longitudinal axis of valve frame. Panel (A) Design of the Venus A-Valve. Panel (B) Distribution of force within the valve frame stratified by aortic valve morphology. Panel (C) Distribution of force within the valve frame stratified by calcification volume. Values presented in median and interquartile range.

Table 1
Pre- and post-procedural MSCT measurements.

		All (n = 20)	Bicuspid aortic valve (n = 10)	Tricuspid aortic valve (n = 10)
Native anatomy				
Annulus	D_{min}, mm	20.6 (5.5)	22.9 (4.5)	18.7 (4.1)
	D_{max}, mm	26.5 (5.1)	26.7 (6.2)	26.2 (4.1)
	Perimeter, mm	73.4 (14.5)	76.6 (19.3)	72.7 (10.5)
	Area, mm^2	407.2 (183.0)	450.9 (239.7)	397.5 (114.3)
	Eccentricity index	1.3 (0.2)	1.2 (0.2)	1.4 (0.1)
	Calcium volume, mm^3	531.5 (695.0)	804.5 (597.3)	361.0 (492.5)
Procedure				
	Perimeter oversizing, %	15.0 (8.2)	12.8 (12.1)	19.3 (9.6)
	Pre-dilatation, n (%)	17 (85%)	10 (100%)	7 (70%)
	Post-dilatation, n (%)	11 (55%)	7 (70%)	4 (40%)
	Depth of implantation, mm	8.1 (4.6)	7.6 (5.1)	8.1 (7.5)
Frame geometry				
Inflow	Eccentricity index	1.1 (0.2)	1.1 (0.3)	1.1 (0.1)
	Expansion, %	77.0 (30.1)	69.5 (34.3)	88.5 (21.7)
Nadir	Eccentricity index	1.2 (0.2)	1.2 (0.2)	1.1 (0.1)
	Expansion, %	81.0 (20.3)	77.7 (18.7)	87.5 (19.7)

(represented by the most significant waist on the valve) was at around 6 mm above the annulus (Xiong et al., 2019). Alternatively, biomechanical interaction can be analyzed from *in to vitro* experiment (Mummert et al., 2013). These approaches, however, are limited since they do not incorporate neither the anatomy nor the physical properties of the patient's anatomy. Yet, this has become possible with patient-specific computer simulation in which the baseline anatomy is derived from the patient's baseline MSCT and during which the detailed anatomic/geometric and mechanical properties of both the device and host are incorporated in the simulation algorithm (Schultz et al., 2016; de Jaegere et al., 2016; Rocatello et al., 2018; Dowling et al., 2019; de Jaegere et al., 2016). We sought to analyze the forces within the transcatheter aortic valves through patient-specific computer simulation in this exploratory study.

2. Material and methods

2.1. Patient population

This is a retrospective, single-center study including 20 patients with aortic stenosis (10 with bicuspid aortic valve [BAV]), who have successfully received TAVR and have MSCT pre- and post-TAVR during the index hospitalization. The first-generation self-expanding Venus A-Valve (Venus MedTech Inc., Hangzhou, China, Fig. 1A) was used (Jilaihawi et al., 2015), which catered to the valve design to provide a stronger radial force. BAV was classified by the TAVR operators on MSCT according to the Sievers system (Sievers and Schmidtke, 2007), as well as a TAVR-directed system (Jilaihawi et al., 2016). Pre-procedural assessment of the aortic root from MSCT was performed with FluoroCT 3.0 (Circle Cardiovascular Imaging Inc., Calgary, Canada). The indication for TAVR was discussed by our multidisciplinary Heart Team. The nadir of bioprosthetic leaflets of Venus A-Valve is at 12.9 mm, 13.6 mm, 16.2 mm and 16.0 mm above the inflow for its 23 mm (total height of 45.9 mm), 26 mm (total height of 49.9 mm), 29 mm (total height of 51.3 mm) and 32 mm (total height of 50.8 mm) valve, respectively. The selection of prosthesis size was based on annular-sizing combined with assessing supra-annular structures and balloon-sizing (Xiong et al., 2018; Xu et al., 2020), left to operator's discretion. The transfemoral approach was the default access. Procedural details of TAVR have been reported (Liao et al., 2018). All patients provided consent for anonymized data acquisition and analysis. The study protocol was approved by our local institutional ethical committee.

2.2. Computer simulation

All MSCT scans were performed with a second-generation dual-source CT system (SIEMENS SOMATOM Definition Flash; SIEMENS Healthcare, Erlangen, Germany) prior to and following TAVR (Guo et al., 2013). Prior to computer simulation, candidate MSCT scans were reviewed to exclude those with significant artifacts or blooming effect that deemed suboptimal for segmentation. Patient-specific computer simulation was performed using FEops HEARTguide technology (FEops NV, Ghent, Belgium), which has been described previously (de Jaegere et al., 2016; Rocatello et al., 2018). All simulations in this current study were conducted with the CE marked version under standard settings (Rocatello et al., 2018). This technique has been shown to be able to predict device-anatomy interaction in detail for both tricuspid and bicuspid aortic stenosis (de Jaegere et al., 2019).

Patient-specific finite element models of the aortic root were constructed from pre-procedural MSCT imaging. The aortic wall, leaflets, and calcium were modeled with differing mechanical properties (Dowling et al., 2019). Calcification was measured at the default threshold of 850 Hounsfield units. For each patient, the position and depth of implantation of the device have been derived from the post-procedural

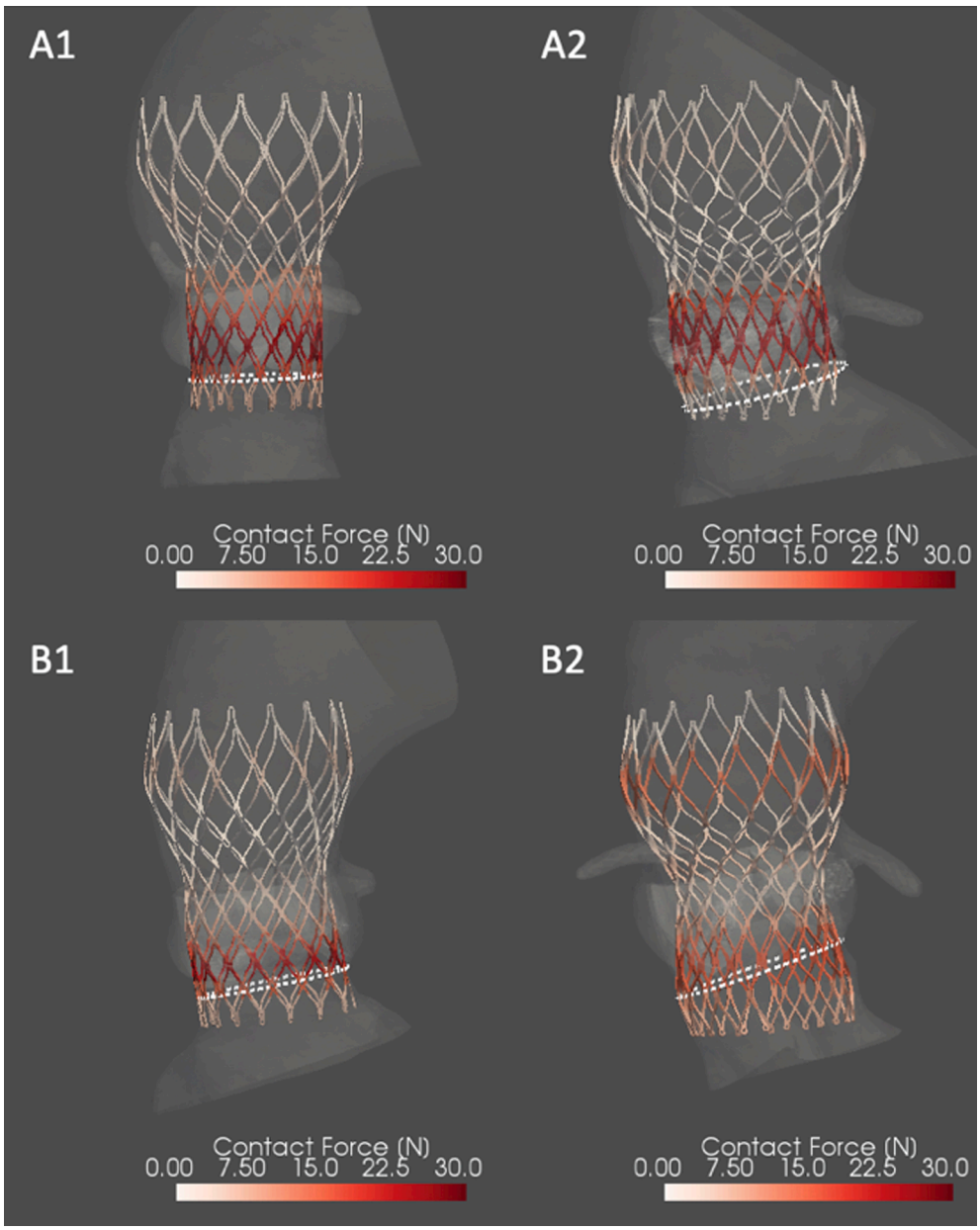

Fig. 2. Representative maps of force within the transcatheter aortic valves in bicuspid and tricuspid aortic valve. Panel (A) 26 mm and 29 mm Venus A-Valve in patients with BAV. Panel (B) 26 mm and 29 mm Venus A-Valve in patients with tricuspid aortic valve.

MSCT, guaranteeing a reliable representation of the actual implant. From the Finite Element Analysis simulation's result, the force values were extracted from the deformed configuration of the valve frame (final step) along the radial direction, representing the force exerted by the device that interacts with the different anatomical structures, being aortic tissue, healthy valve tissue or calcified tissue. Rotational alignment was not included in the modelling process. The frame was divided every 3 mm along with its longitudinal axis, and every 22.5° along the circumferential direction, leading to 288 sectors, wherein the nodal forces were summed, obtaining the values used in the present analysis.

Angulation exists between the long axis of valve frame and aortic root. When comparing the native structures of the level of maximal force and the native annulus, we resliced the frame at the same height but parallel to the annulus for simplification. The modification is more relevant to clinical practice since we assess the intra-leaflet structures following the long axis of the aortic root. At the level of maximal force, a further qualitative analysis was done to delineate possible anatomical features that exerted significant force to the frame, as well as the calculation of dimensional changes from the annulus to the 'supra-annulus' (i.e. the shape and size of the valve frame at the level of maximal force).

2.3. Frame geometry

Frame geometry on post-procedural MSCT was assessed at the frame inflow and at the nadir of bioprosthetic leaflet. Eccentricity index was calculated as the ratio of maximum and minimum diameter (Tchetche et al., 2019). Frame expansion was determined as actual area/nominal area × 100% (Kazuno et al., 2016).

2.4. Statistical analysis

Continuous variables are presented as median (interquartile range, IQR). Categorical variables are presented as frequencies and

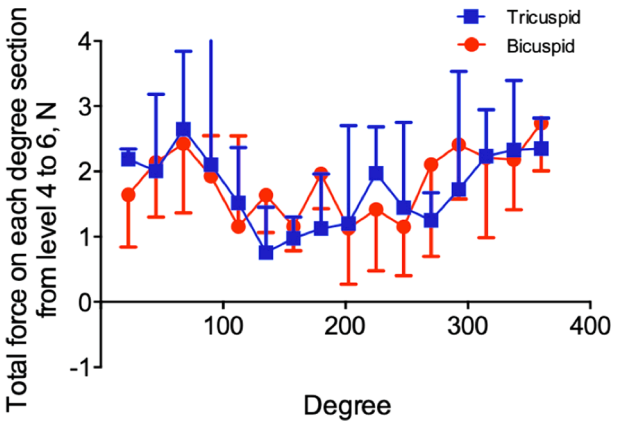

Fig. 3. Distribution of force on the short axis of valve frame from level 4 to 6. Values presented in median and interquartile range.

percentages. Given the nature and objective of study (assessment of force within valve in a small sample of patients, in which data will be shown for all and two small subgroups), no formal statistical analyses have been performed.

3. Results

3.1. Baseline, procedural details and MSCT measurements

The median age was 72.5 (IQR: 9.0) years and 9 were females. Of the 10 patients with BAV, three were classified as Type 1 and the other 7 as Type 0 (i.e. 1 bicommissural raphe-type with coronary cusp fusion, 2 tricommissural type and 7 bicommissural non raphe-type). The Pre- and post-procedural MSCT measurements are summarized in Table 1. Patients with BAV had a larger annulus with a larger amount of calcification than tricuspid aortic valve (TAV) patients but with similar annular eccentricity. Depth of implantation was similar but despite a higher frequency of pre- and post-dilatation, the frame was less expanded in BAV than TAV patients at the inflow and nadir but with similar eccentricity of the frame. The transaortic gradient decreased from 57 (IQR: 27) mmHg to 12 (IQR: 8) mmHg. No patient had more than mild PVL but 3 patients underwent permanent pacemaker implantation before discharge.

3.2. Distribution of force within Venus valve frame

The total force on the frame in all patients was 74.9 (IQR: 24.0) N, 68.5 (IQR: 27.5) N in BAV and 74.9 (IQR: 20.7) N in TAV respectively. A representative map of force in BAV and TAV patients is shown in Fig. 2. The distribution of force within the valve frame on its longitudinal axis is shown in Fig. 1B and 1C. In all patients, the maximal force (F-max) was located at level 5 corresponding with the nadir of the bioprosthetic leaflets (9.9 [IQR: 7.1] N, 10.3 [IQR: 6.6] N in BAV and 9.7 [IQR: 9.2] N

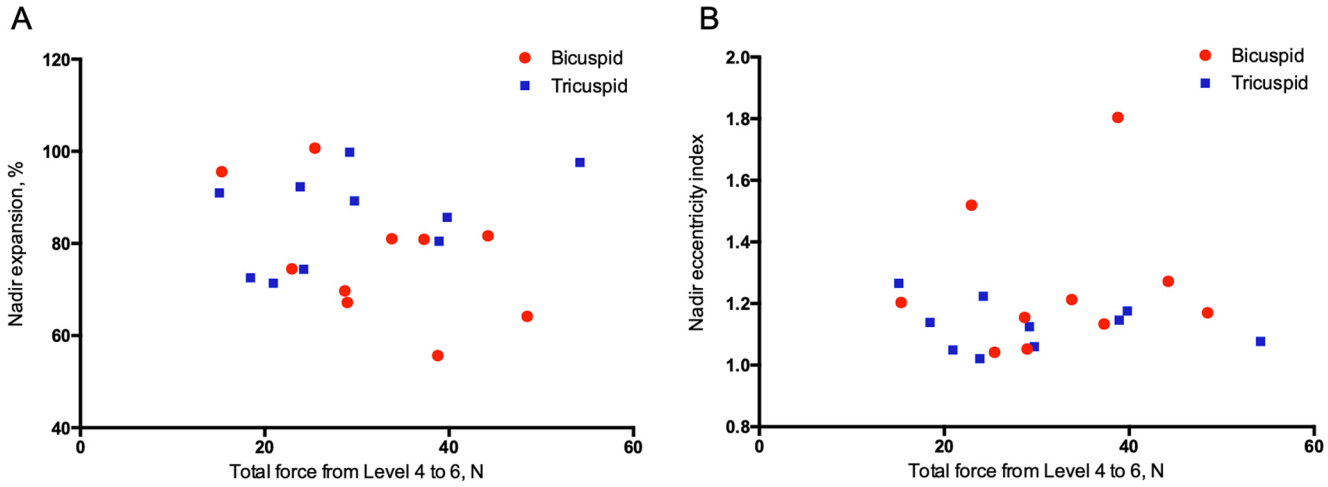

Fig. 4. Scatter plot illustrating relationship between the total force (level 4–6) and frame geometry at the level 5 (i.e. nadir of bioprosthetic leaflets). Panel (A) Scatter plot between the sum of force from level 4 to 6 and frame expansion at the level of nadir. Panel (B) Scatter plot between the sum of force from level 4 to 6 and frame eccentricity at the level of nadir.

Fig. 5. Cross-sectional view illustrating the displacement of the native structures of the aortic root at the level of maximal force on valve frame. Calcium in grey and leaflet tissue in pink. The yellow dot represents the location of maximal force. (For interpretation of the references to colour in this figure legend, the reader is referred to the web version of this article.)

in TAV). A second peak of force was located at the outflow area of the valve. The distance of the level of F-max and annulus was greater in BAV than TAV patients (8.8 [IQR: 4.8] vs. 1.8 [IQR: 7.4] mm, Fig. 1B) but BAV patients had a somewhat higher depth of implantation (Table 1). Patients with greater calcium volume (i.e. > 530 mm^3, n = 9) had numerically larger force at level 5 than patients with smaller calcification volume (12.8 [IQR: 7.4] vs. 9.8 [IQR: 4.5] N, Fig. 1C). Fig. 3 shows that the distribution of force (level 4–6) along the cross section of the valve frame at the prespecified 22.5° increment is inhomogeneous. The relation between total force from level 4 to 6 and frame geometry (expansion and eccentricity) at nadir of bioprosthetic leaflets is illustrated in Fig. 4.

3.3. Displacement of native structures

Displacement of native aortic root structures at the level of maximal force on the valve frame is illustrated in Fig. 5. The point of maximal force on the level (i.e. the yellow dot) located either at a calcium deposit, commissure or aortic wall. The valve frame in patients with TAV pushed the native anatomy all the way to aortic wall more often than in patients with BAV. The difference in dimension of the valve frame from annulus to the level of F- max (i.e. the dimension at annulus minus the dimension at F-max) was more pronounced in BAV than TAV patients (perimeter: 5.7 [IQR: 6.2] mm vs. −0.4 [IQR: 3.7] mm; area: 73.8 [IQR: 97.1] mm^2 vs. −17.7 [IQR: 33.8] mm^2), forming a tapered shape between the two planes in BAV but tubular in TAV patients.

4. Discussion

The main findings of this study, using patient-specific computer simulation to assess the force within the Venus valve after TAVR, are that most of the force within the bioprosthesis is seen at the level corresponding with the nadir of bioprosthetic leaflets and is unequally distributed along the cross-sectional axis. Calcium volume did not alter the pattern of force distribution on the longitudinal axis of the frame, but more calcium translated to larger force. A more pronounced tapering of the valve frame was observed from annulus to the area of F-max and, hence, a lesser degree of expansion in patients with BAV (higher calcium load) despite more frequent pre- and post-dilatation and a higher degree of oversizing than in patients with TAV. These findings stem from a small single-center observational study that precludes firm conclusions and in particular a valid comparison between patients with BAV and TAV. Clinical consequences of the findings are left to be further studied.

Although the mutual force exerted by the valve on host tissue and vice versa has never been studied in patient-specific anatomy, this force is pivotal for proper anchoring of the prosthesis. Also, it is customary in clinical practice to select a valve that is a bit larger than the native annulus (i.e. oversizing) to ensure anchoring and to minimize PVL. Consequently, the force on both the valve and tissue may unintentionally increase that in turn may affect frame and leaflet integrity, represented by frame under-expansion or ellipticity (Tchetche et al., 2019), and also may be associated with clinical complications such as structural valve deterioration due to the link between under-expansion and hypo-attenuated leaflet thickening (Fuchs et al., 2017). The understanding of the force distribution may serve to propose more refined sizing strategies and, hence, less mechanical stress on prosthesis and host, thereby improving durability and safety of TAVR (Xuan et al., 2020). The data of this analysis demonstrate the mechanical interaction between the valve frame and the base of the aortic root that includes the native leaflet. Since these leaflets are not excised during TAVR, they also contribute to the force generation within the valve frame. To what extent the annulus itself and other structures of the aortic root such as the native leaflets contribute to the force generation is unknown. Conceptually, this will vary from patient to patient depending to dimensions, morphology and calcium load of annulus and leaflets.

This is in line with proposals to include supra-annular structures of the aortic root in addition to the dimensions of the annulus itself for sizing in patients with BAV (Iannopollo et al., 2020; Iannopollo et al., 2019; Petronio et al., 2020; Xiong et al., 2018). Acknowledging the small-scale observational nature of this study, we found that the valve frame mobilized the supra-annular structures to a lesser extent in BAV than in TAV patients. Also, the decrease in dimension of the bioprosthetic valve frame from inflow to level of F-max was more pronounced, resulting in a lesser degree of expansion in BAV patients. It supports a tailored sizing strategy in BAV morphology (Tarantini and Fabris, 2021). Conceptually, this may also hold for TAV patients with significant leaflet calcification. While in a preliminary state, patient-specific computer simulation also showed promise to guide sizing in both morphologies (Dowling et al., 2021; Dowling et al., 2020; El Faquir et al., 2020).

The understanding of the force distribution within the valve frame may be of particular value for self-expanding bioprostheses such as the Medtronic Evolut platforms and the Venus valve used in this study. Their design is such that the inflow portion containing the skirt to prevent PVL is anchored in the base of the aortic root while the bioprosthetic leaflets are in a supra-annular position in relation to the patient's annulus. For instance, the Evolut PRO valve has a skirt with a height of 13 mm and requires a certain depth of implantation (in general at least 2–4 mm below the patient's annulus) to ensure coronary patency (Yudi et al., 2018). Based upon the findings in this study that the level of F-max exerted on the frame is at 6–8 mm above the annulus and given an ideal position of the nadir of bioprosthetic leaflets at 6 mm above the annulus, the depth of implantation should not exceed 5–7 mm. The findings, thus, support the current practice that considers depth of implantation of 4–6 mm as optimal for self-expanding valves.

The main limitations of this study are its small-scale single center nature and the retrospective selection of patients. It was underpowered to perform formal statistical tests. A larger sample with a more comprehensive data set would allow the analysis of the determinants of force including aortic valve morphology plus the effects of force on long-term valve and leaflet integrity/function. The retrospective nature affects generalizability and external validity. Also, the data pertain to the self-expanding Venus A-Valve. The applicability to other devices must be confirmed.

5. Conclusions

Patient-specific finite element analysis helps to visualize and delineate prosthesis-anatomy interactions after TAVR, thereby providing insights into improving TAVR planning and subsequently long-term outcome. Most of the force exerted by the anatomy was located at the level of the nadir of the bioprosthetic leaflets, higher than the native annulus. In patients with BAV, this was associated with a more pronounced tapering in space from the annulus and less expansion of the frame than TAV morphology.

Funding

This work was supported by National Natural Science Foundation of China (82102129), the European Union's Horizon 2020 research and innovation program (945698), the fellowship of China Postdoctoral Science Foundation (2020M683327) and Open Fund Research from State Key Laboratory of Hydraulics and Mountain River Engineering (SKHL1920).

Declaration of Competing Interest

The authors declare the following financial interests/personal relationships which may be considered as potential competing interests: Yuan Feng and Mao Chen are proctors/consultants of Venus MedTech. Elisa Stoppani and Matthieu De Beule are employees of Feops NV. The other authors report no disclosures.

References

Bailey, J., Curzen, N., Bressloff, N.W., 2017. The impact of imperfect frame deployment and rotational orientation on stress within the prosthetic leaflets during transcatheter aortic valve implantation. J. Biomech. 53, 22–28. https://doi.org/10.1016/j.jbiomech.2016.12.031.

Blanke, P., Willson, A.B., Webb, J.G., Achenbach, S., Piazza, N., Min, J.K., Pache, G., Leipsic, J., 2014. Oversizing in transcatheter aortic valve replacement, a commonly used term but a poorly understood one: dependency on definition and geometrical measurements. J. Cardiovasc. Comput. Tomogr. 8 (1), 67–76. https://doi.org/10.1016/j.jcct.2013.12.020.

de Jaegere, P., De Santis, G., Rodriguez-Olivares, R., Bosmans, J., Bruining, N., Dezutter, T., Rahhab, Z., El Faquir, N., Collas, V., Bosmans, B., Verhegghe, B., Ren, C., Geleinse, M., Schultz, C., van Mieghem, N., De Beule, M., Mortier, P., 2016. Patient-specific computer modeling to predict aortic regurgitation after transcatheter aortic valve replacement. JACC Cardiovasc. Interv. 9 (5), 508–512. https://doi.org/10.1016/j.jcin.2016.01.003.

de Jaegere, P., Rocatello, G., Prendergast, B.D., de Backer, O., Van Mieghem, N.M., Rajani, R., 2019. Patient-specific computer simulation for transcatheter cardiac interventions: what a clinician needs to know. Heart Br. Card. Soc. 105 (Suppl 2), s21–s27. https://doi.org/10.1136/heartjnl-2018-313514.

Dowling, C., Bavo, A.M., El Faquir, N., Mortier, P., de Jaegere, P., De Backer, O., Sondergaard, L., Ruile, P., Mylotte, D., McConkey, H., Rajani, R., Laborde, J.-C., Brecker, S.J., 2019. Patient-specific computer simulation of transcatheter aortic valve replacement in bicuspid aortic valve morphology. Circ. Cardiovasc. Imaging 12, e009178. https://doi.org/10.1161/CIRCIMAGING.119.009178.

Dowling, C., Firoozi, S., Brecker, S.J., 2020. First-in-human experience with patient-specific computer simulation of TAVR in bicuspid aortic valve morphology. JACC Cardiovasc. Interv. 13 (2), 184–192. https://doi.org/10.1016/j.jcin.2019.07.032.

Dowling, C., Gooley, R., McCormick, L., Firoozi, S., Brecker, S.J., 2021. Patient-specific computer simulation: an emerging technology for guiding the transcatheter treatment of patients with bicuspid aortic valve. Interv. Cardiol. Rev. Res. Resour. 16, e26. https://doi.org/10.15420/icr.2021.09.

El Faquir, N., De Backer, O., Bosmans, J., Rudolph, T., Buzzatti, N., Bieliauskas, G., Collas, V., Wienemann, H., Schiavi, D., Cummins, P., Rahhab, Z., Kroon, H., Wolff, Q., Lenzen, M., Ribeiro, J.M., Latib, A., Adam, M., Søndergaard, L., Ren, B., Van Mieghem, N., de Jaegere, P., 2020. Patient-specific computer simulation in TAVR with the self-expanding evolut R valve. JACC Cardiovasc. Interv. 13, 1803–1812. https://doi.org/10.1016/j.jcin.2020.04.018.

Fuchs, A., De Backer, O., Brooks, M., de Knegt, M.C., Bieliauskas, G., Yamamoto, M., Yanagisawa, R., Hayashida, K., Sondergaard, L., Kofoed, K.F., 2017. Subclinical leaflet thickening and stent frame geometry in self-expanding transcatheter heart valves. Eurointervent. J. Eur. Collab Work. Group Interv. Cardiol. Eur. Soc. Cardiol. 13, e1067–e1075. https://doi.org/10.4244/EIJ-D-17-00373.

Gunning, P.S., Vaughan, T.J., McNamara, L.M., 2014. Simulation of self expanding transcatheter aortic valve in a realistic aortic root: implications of deployment geometry on leaflet deformation. Ann. Biomed. Eng. 42 (9), 1989–2001. https://doi.org/10.1007/s10439-014-1051-3.

Guo, Y.-K., Yang, Z.-G., Shao, H., Deng, W., Ning, G., Dong, Z.-H., 2013. Right ventricular dysfunction and dilatation in patients with mitral regurgitation: analysis using ECG-gated multidetector row computed tomography. Int. J. Cardiol. 167 (4), 1585–1590. https://doi.org/10.1016/j.ijcard.2012.04.104.

Iannopollo, G., Romano, V., Buzzatti, N., Ancona, M., Ferri, L., Russo, F., Bellini, B., Granada, J.F., Chieffo, A., Montorfano, M., 2020. Supra-annular sizing of transcatheter aortic valve prostheses in raphe-type bicuspid aortic valve disease: the LIRA method. Int. J. Cardiol. 317, 144–151. https://doi.org/10.1016/j.ijcard.2020.05.076.

Iannopollo, G., Romano, V., Buzzatti, N., De Backer, O., Søndergaard, L., Merkely, B., Prendergast, B.D., Giannini, F., Colombo, A., Latib, A., Granada, J.F., Chieffo, A., Montorfano, M., 2019. A novel supra-annular plane that predicts TAVI prosthesis anchoring in raphe-type bicuspid aortic valve disease: the LIRA plane. EuroIntervent. J. Eur. Collab. Work. Group Interv. Cardiol. Eur. Soc. Cardiol. https://doi.org/10.4244/EIJ-D-19-00951.

Jatene, M.B., Monteiro, R., Guimaraes, M.H., Veronezi, S.C., Koike, M.K., Jatene, F.B., Jatene, A.D., 1999. Aortic valve assessment. Anatomical study of 100 healthy human hearts. Arq. Bras. Cardiol. 73, 75–86.

Jilaihawi, H., Chen, M., Webb, J., Himbert, D., Ruiz, C.E., Rodés-Cabau, J., Pache, G., Colombo, A., Nickenig, G., Lee, M., Tamburino, C., Sievert, H., Abramowitz, Y., Tarantini, G., Alqoofi, F., Chakravarty, T., Kashif, M., Takahashi, N., Kazuno, Y., Maeno, Y., Kawamori, H., Chieffo, A., Blanke, P., Dvir, D., Ribeiro, H.B., Feng, Y., Zhao, Z.-G., Sinning, J.-M., Kliger, C., Giustino, G., Pajerski, B., Imme, S., Grube, E., Leipsic, J., Vahanian, A., Michev, I., Jelnin, V., Latib, A., Cheng, W., Makkar, R., 2016. A bicuspid aortic valve imaging classification for the TAVR era. JACC Cardiovasc. Imag. 9 (10), 1145–1158. https://doi.org/10.1016/j.jcmg.2015.12.022.

Jilaihawi, H., Wu, Y., Yang, Y., Xu, L., Chen, M., Wang, J., Kong, X., Zhang, R., Wang, M., Lv, B., Wang, W., Xu, B., Makkar, R.R., Sievert, H., Gao, R., 2015. Morphological characteristics of severe aortic stenosis in China: imaging corelab observations from the first Chinese transcatheter aortic valve trial. Catheter. Cardiovasc. Interv. Off. J. Soc. Card. Angiogr. Interv. 85 (Suppl 1), 752–761. https://doi.org/10.1002/ccd.25863.

Kazuno, Y., Maeno, Y., Kawamori, H., Takahashi, N., Abramowitz, Y., Babak, H., Kashif, M., Chakravarty, T., Nakamura, M., Cheng, W., Friedman, J., Berman, D., Makkar, R.R., Jilaihawi, H., 2016. Comparison of SAPIEN 3 and SAPIEN XT transcatheter heart valve stent-frame expansion: evaluation using multi-slice computed tomography. Eur. Heart J. Cardiovasc. Imag. 17 (9), 1054–1062. https://doi.org/10.1093/ehjci/jew032.

Liao, Y., Li, Y., Xiong, T., Ou, Y., Lv, W., He, J., Li, Y.-M., Zhao, Z., Wei, X., Xu, Y., Feng, Y., Chen, M., 2018. Comparison of procedural, clinical and valve performance results of transcatheter aortic valve replacement in patients with bicuspid versus tricuspid aortic stenosis. Int. J. Cardiol. 254, 69–74. https://doi.org/10.1016/j.ijcard.2017.12.013.

Mummert, J., Sirois, E., Sun, W., 2013. Quantification of biomechanical interaction of transcatheter aortic valve stent deployed in porcine and ovine hearts. Ann. Biomed. Eng. 41 (3), 577–586. https://doi.org/10.1007/s10439-012-0694-1.

Petronio, A.S., Angelillis, M., De Backer, O., Giannini, C., Costa, G., Fiorina, C., Castriota, F., Bedogni, F., Laborde, J.C., Søndergaard, L., 2020. Bicuspid aortic valve sizing for transcatheter aortic valve implantation: development and validation of an algorithm based on multi-slice computed tomography. J. Cardiovasc. Comput. Tomogr. 14 (5), 452–461. https://doi.org/10.1016/j.jcct.2020.01.007.

Rocatello, G., El Faquir, N., De Santis, G., Iannaccone, F., Bosmans, J., De Backer, O., Sondergaard, L., Segers, P., De Beule, M., de Jaegere, P., Mortier, P., 2018. Patient-specific computer simulation to elucidate the role of contact pressure in the development of new conduction abnormalities after catheter-based implantation of a self-expanding aortic valve. Circ. Cardiovasc. Interv. 11, e005344. https://doi.org/10.1161/CIRCINTERVENTIONS.117.005344.

Schultz, C., Rodriguez-Olivares, R., Bosmans, J., Lefèvre, T., De Santis, G., Bruining, N., Collas, V., Dezutter, T., Bosmans, B., Rahhab, Z., El Faquir, N., Watanabe, Y., Segers, P., Verhegghe, B., Chevalier, B., van Mieghem, N., De Beule, M., Mortier, P., de Jaegere, P., 2016. Patient-specific image-based computer simulation for theprediction of valve morphology and calcium displacement after TAVI with the Medtronic CoreValve and the Edwards SAPIEN valve. EuroIntervention 11 (9), 1044–1052. https://doi.org/10.4244/EIJV11I9A212.

Sievers, H.-H., Schmidtke, C., 2007. A classification system for the bicuspid aortic valve from 304 surgical specimens. J. Thorac. Cardiovasc. Surg. 133 (5), 1226–1233. https://doi.org/10.1016/j.jtcvs.2007.01.039.

Tarantini, G., Fabris, T., 2021. Transcatheter aortic valve replacement for bicuspid aortic valve stenosis: a practical operative overview. Circ. Cardiovasc. Interv. 14 (7) https://doi.org/10.1161/CIRCINTERVENTIONS.120.009827.

Tchetche, D., de Biase, C., van Gils, L., Parma, R., Ochala, A., Lefevre, T., Hovasse, T., De Backer, O., Sondergaard, L., Bleiziffer, S., Lange, R., Kornowski, R., Landes, U., Norgaard, B.L., Biasco, L., Philippart, R., Molina-Martin de Nicolas, J., Mylotte, D., Lemee, C., Dumonteil, N., Van Mieghem, N.M., 2019. Bicuspid aortic valve anatomy and relationship with devices: the BAVARD multicenter registry. Circ. Cardiovasc. Interv. 12, e007107. https://doi.org/10.1161/CIRCINTERVENTIONS.118.007107.

Xiong, T.-Y., Feng, Y., Li, Y.-J., Zhao, Z.-G., Liao, Y.-B., Ou, Y., Wei, X., Chen, M., 2018. Supra-annular sizing for transcatheter aortic valve replacement candidates with bicuspid aortic valve. JACC Cardiovasc. Interv. 11 (17), 1789–1790. https://doi.org/10.1016/j.jcin.2018.06.002.

Xiong, T.-Y., Li, Y.-J., Feng, Y., Liao, Y.-B., Zhao, Z.-G., Mylotte, D., Wei, X., Xu, Y.-N., Peng, Y., Wei, J.-F., Zheng, M.-X., Zhou, X., Meng, W., Piazza, N., Chen, M., 2019. Understanding the interaction between transcatheter aortic valve prostheses and supra-annular structures from post-implant stent geometry. JACC Cardiovasc. Interv. 12 (12), 1164–1171. https://doi.org/10.1016/j.jcin.2019.02.051.

Xu, Y.-N., Xiong, T.-Y., Li, Y.-J., Liao, Y.-B., Zhao, Z.-G., Wei, X., Feng, Y., Chen, M., 2020. Balloon sizing during transcatheter aortic valve implantation: comparison of different valve morphologies. Herz 45 (2), 192–198. https://doi.org/10.1007/s00059-018-4714-2.

Xuan, Y., Dvir, D., Wang, Z., Ye, J., Guccione, J.M., Ge, L., Tseng, E.E., 2020. Stent and leaflet stresses across generations of balloon-expandable transcatheter aortic valves. Interact. Cardiovasc. Thorac. Surg. 30, 879–886. https://doi.org/10.1093/icvts/ivaa037.

Yudi, M.B., Sharma, S.K., Tang, G.H.L., Kini, A., 2018. Coronary angiography and percutaneous coronary intervention after transcatheter aortic valve replacement. J. Am. Coll. Cardiol. 71, 1360–1378. https://doi.org/10.1016/j.jacc.2018.01.057.

Zegdi, R., Ciobotaru, V., Noghin, M., Sleilaty, G., Lafont, A., Latrémouille, C., Deloche, A., Fabiani, J.-N., 2008. Is it reasonable to treat all calcified stenotic aortic valves with a valved stent? Results from a human anatomic study in adults. J. Am. Coll. Cardiol. 51 (5), 579–584. https://doi.org/10.1016/j.jacc.2007.10.023.